

Influence of molecular temperature on the coherence of fullerenes in a near-field interferometerKlaus Hornberger,^{1,2} Lucia Hackermüller,¹ and Markus Arndt^{1,*}¹*Institut für Experimentalphysik, Universität Wien, Boltzmanngasse 5, A-1090 Wien, Austria*²*Department für Physik, Universität München, Theresienstraße 37, D-80333 München, Germany*

(Received 23 September 2004; published 3 February 2005)

We study C₇₀ fullerene matter waves in a Talbot-Lau interferometer as a function of their temperature. While the ideal fringe visibility is observed at moderate molecular temperatures, we find a gradual degradation of the interference contrast if the molecules are heated before entering the interferometer. A method is developed to assess the distribution of the microcanonical temperatures of the molecules in free flight. This way the heating-dependent reduction of interference contrast can be compared with the predictions of quantum theory. We find that the observed loss of coherence agrees quantitatively with the expected decoherence rate due to the thermal radiation emitted by the hot molecules.

DOI: 10.1103/PhysRevA.71.023601

PACS number(s): 03.75.-b, 03.65.Yz

I. INTRODUCTION

The wave-particle duality of material objects is a hallmark of quantum mechanics. Up to now, the wave nature of particles has been demonstrated for electrons, neutrons, atoms, and coherent atomic ensembles. Recently, even the interference of composite objects has been observed ranging from molecular dimers [1–3] and van der Waals clusters [4] to fullerenes [5], massive fullerene derivatives, and small biomolecules [6]. In particular, the advances with large molecules have stimulated the question of what determines the limits to observe quantum delocalization with massive objects.

From the theoretical side, there is also an increased interest concerning the location of the apparent quantum-classical boundary. The recent understanding of decoherence phenomena points to the crucial role played by the environmental interaction in determining whether a quantum particle shows wave behavior [7].

Several experiments tackled this issue in the context of interferometry. Pritchard and co-workers studied the loss of interference contrast in an atom interferometer where sodium atoms were subjected to resonant laser light [8,9]. The photons emitted in a spontaneous decay then both imparted a recoil on the atom and entangled the atomic state with the escaping photon state. Similarly, the Brune *et al.* experiment [10] can be regarded as an internal state interferometer, where the fringe visibility depends on the entanglement between the atom and the field mode of the emitted photon [11]. Decoherence has also been investigated in a Mach-Zehnder interferometer with a two-dimensional electron gas in a semiconductor heterostructure [12]. Heiblum and co-workers observed a loss of fringe visibility when the mesoscopic structure was heated.

Here, we describe in detail our recent molecule interferometry experiment which explores the loss of fringe contrast when the internal degrees of freedom of fullerene molecules

are heated to temperatures above 2000 K. It is based on the fact that hot fullerenes emit thermal, visible light in a continuous spectrum [13]. One expects that the emitted photons will reduce the fringe contrast once they are energetic enough to perturb the motional state of the molecule, or equivalently, if they convey sufficient information about its position [14]. While the original observation has been published in [15], the present article provides a detailed account of the experimental and theoretical techniques used to determine the temperature of the fullerenes in free flight, which is needed to calculate the expected decoherence effect.

In Sec. II we describe the setup of the experiment and our method for varying the molecular temperature by laser heating. Section III provides a quantitative description of the thermally emitted radiation, which determines the localization of the molecular waves and their cooling process. Knowledge of the latter is required in Sec. IV where a model is presented that quantifies the competing dynamics between ionization and cooling of the fullerenes. The comparison with experimental data in Sec. V allows us to extract the temperature distribution in the beam. In Sec. VI we compare the observed loss of visibility to the expectations from quantum theory, and we discuss alternative decoherence mechanisms in Sec. VII.

II. INTERFEROMETRY WITH HEATED FULLERENES**A. The interferometer**

We use a Talbot-Lau matter wave interferometer as already described in detail in [16]. It consists of three gold gratings with a period of $d=990$ nm and a nominal open width of 470 nm which are equally separated by the distance $L=38$ cm; see Fig. 1. The first grating of the setup prepares the wave coherence in the beam. Near-field diffraction at the second grating then produces a high-contrast interference pattern at the position of the third grating provided the grating separation L is close to a multiple of the Talbot length $L_T=d^2/\lambda_{C70}$ [17]. At a grating separation of $L=0.38$ m the interference fringes corresponding to the first and the second Talbot orders are expected at molecular de Broglie wavelengths of $\lambda_{C70}=2.6$ and 5.2 pm, respectively. Different

*Author to whom correspondence should be addressed. Electronic address: markus.arndt@univie.ac.at

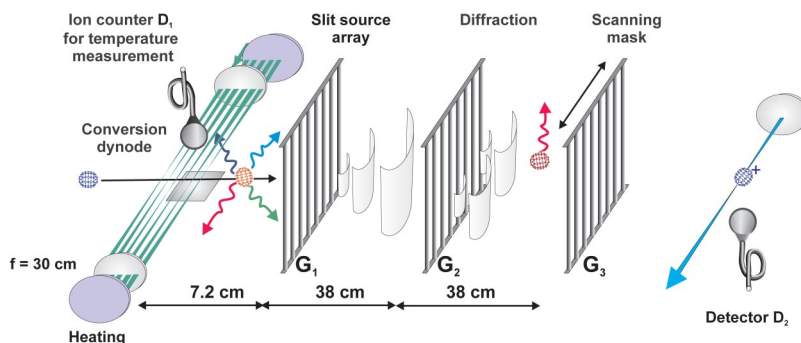


FIG. 1. The Talbot-Lau interferometer consists of three equal gratings with a slit separation of $d=0.99 \mu\text{m}$ spaced by a distance of $L=38 \text{ cm}$. The interference contrast can be reduced by heating the fullerenes in front of the interferometer via multiple laser beams.

height constrictions are used to select the required velocities centered at 100 m/s ($\Delta v/v \approx 10\%$) and at 190 m/s ($\Delta v/v \approx 15\%$) out of a thermal beam of fullerenes, which is produced by sublimation at a temperature of 900 K . The interference pattern has a period equal to the grating constant d . Therefore one observes modulation fringes in the transmitted flux I if the third grating is shifted laterally. The transmitted molecules are detected behind the third grating by laser ionization. The observed contrast of the fringe signal and its wavelength dependence then prove unambiguously the coherence of the interference effect.

As shown in earlier work [6,16] the Talbot-Lau setup is well suited for investigating the wave nature of large molecules such as fullerenes, tetraphenylporphyrins, and fluoro-fullerenes. As an example, Fig. 2 gives the interference signal of C_{70} fullerenes as observed without additional heating. The sinusoidal fringes show the expected visibility $V=(I_{\text{max}}-I_{\text{min}})/(I_{\text{max}}+I_{\text{min}})$ of 47%.

B. The heating stage

This interferometric setup is now complemented by a heating stage about 1 m behind the oven and 7 cm in front of the first grating. It serves to vary the internal energy of the molecules by photon absorption [6]. The green fraction of an argon ion laser ($\lambda=514 \text{ nm}$) is used for the heating stage, while the blue line ($\lambda=488 \text{ nm}$) serves the postionization in the detector. The green line can reach a maximal power of

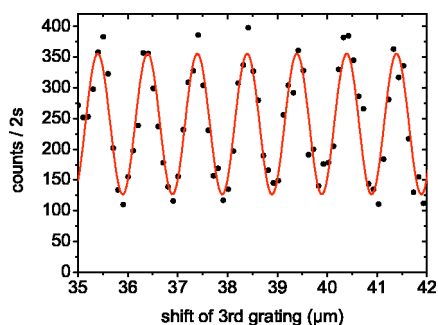


FIG. 2. High-contrast Talbot-Lau interference fringes are observed for fullerenes at temperatures below 1000 K . The fringe visibility of 47% corresponds to the quantum mechanical expectation, indicating coherent molecular evolution.

$P_0=10.8 \text{ W}$ and is focused by a lens of 30 cm focal length to a waist of $w_y=50 \mu\text{m}$. The beam passes a cat-eye arrangement of two lenses and two mirrors under small angles and can thus interact up to 16 times with the molecular beam, as shown in Fig. 1. The distance between the foci of the laser beams is approximately 0.3 mm on average. The beam undergoes some attenuation due to some absorption and reflection in the optical elements. The power after the N th reflection is measured to be about $P_N=11.2-0.42 N \text{ W}$. The power of the blue-detecting laser beam is fixed to 16 W and focused to a waist of $w_y=8 \mu\text{m}$.

The overlap of the laser beam with the molecular beam is monitored by the count rate at detector D_2 , which shows a maximum for an optimal overlap. All heating beams are then adjusted one after the other with respect to maximal increase in the count rate. Molecules which are heated in front of the interferometer maintain much of their internal energy until they reach the detector behind the interferometer. Since the latter is based on thermal ionization [18,19] an increase of the internal molecular energy leads to an enhanced ionization efficiency in the final detection stage. With a molecular beam height of $150 \mu\text{m}$ and a heating laser beam waist of $50 \mu\text{m}$ we are sure that the laser beams overlaps with the molecular beam as long as we can detect an increase for each additional laser beam.

C. Laser heating of fullerenes

Fullerenes are particularly well suited for studying temperature effects in molecular interference since their cage structure provides them with an extraordinary stability against fragmentation. This allows us to deposit more than 100 eV in a single molecule for a sufficiently long time. Laser excitation of these molecules has been studied extensively in the literature; see [20] and references therein. Compared to the more symmetric C_{60} molecule there are fewer symmetry restrictions for dipole transitions in C_{70} . As a result the absorption cross section of C_{70} exceeds that of C_{60} by almost an order of magnitude. This is the main reason for our preference of the C_{70} molecule.

According to Ref. [20] the absorption of a 514 nm photon from the electronic ground state S_0 will excite the singlet state S_1 . This is followed by a rapid nonradiative transition to the metastable triplet state T_1 (the branching ratio exceeds

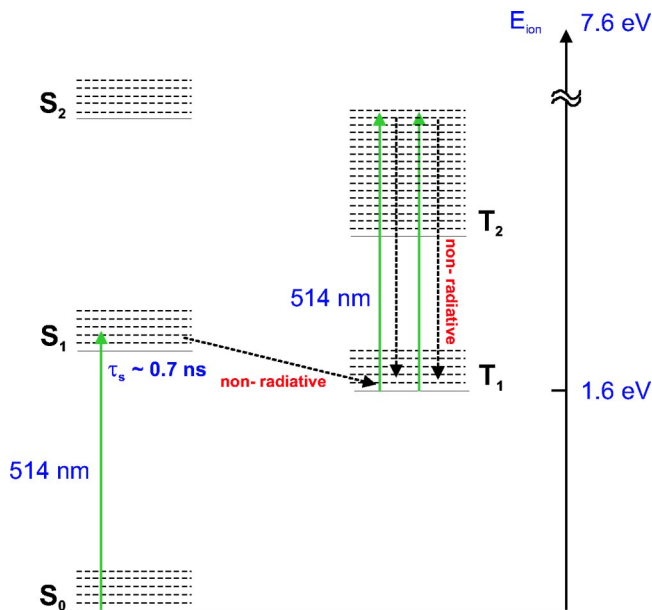


FIG. 3. Electronic excitation energies of C₇₀ [20]. The first photon excites the S₁ state followed by a rapid nonradiative conversion to the relatively long-lived triplet state T₁. All further photon absorption takes place in the electronic triplet configuration.

90%). The relevant energy levels and transitions are summarized in Fig 3. Given the relatively long lifetime of T₁ and the short lifetimes of the other triplet states it is plausible that all further excitation after the first photon occurs sequentially from T₁. The corresponding photon energies absorbed from the heating beam are rapidly transferred to the 204 vibrational degrees of freedom of the molecule. The molecules take about 0.4 ms after the last heating beam until they enter the interferometer.

For fullerenes there are several processes that lead to a loss of the energy stored in the vibrational degrees of freedom. The first relevant mechanism, which is dominant at large internal energies, is thermal emission of radiation. It was observed by several groups that laser heated fullerenes emit visible light in a continuous spectrum [13,21,22]. The form of this spectrum and its dependence on the internal energy determines both the cooling and the decoherence of the molecules, and it is discussed in detail in the next section.

An important competing process is the thermionic emission of electrons. This effect was observed in Ref. [18] and forms the basis of our detection method [23]. Moreover, the thermal ions in the heating stage also provide important information for the assessment of the stored energy of the molecules.

A third thermally activated process, the emission of carbon dimers, can be safely disregarded in our experiment since the ground state fragmentation energy is 10.6 eV [24], while the corresponding ionization potential is 7.6 eV. This energy difference is considerably larger than the maximal energy per vibrational mode in our experiment of about 0.5 eV. As expected, we do not observe any fullerene fragments such as C₆₈ in a quadrupole mass spectrometer mounted behind the interferometer.

By varying the power of the heating laser beam, our setup allows us to control the internal energy of the fullerenes

stored in the vibrational motion of the carbon nuclei. In order to quantify the decoherence caused by the corresponding heat radiation a detailed understanding of the radiative cooling process is indispensable. It is developed in the next section. After that, in Sec. IV, we show how to describe the competing dynamics between the cooling process and the thermal ionization.

III. RADIATIVE COOLING

The 204 vibrational modes of C₇₀ fullerenes form a heat reservoir that can store large amounts of energy. Irrespective of the type of heating, it is sufficient for our purposes to characterize the vibrational state of the molecule by the total internal energy E . Moreover, it is convenient to specify E in terms of a temperature, even though the molecules are insulated from any external heat bath. This can be done by the microcanonical temperature $T(E)=[\partial S/\partial E]^{-1}$, which is defined through the entropy $S(E)$. To leading order, T is the temperature of a fictitious heat bath that would be required to keep the average internal energy of the particle at a value of E .

In free flight the loss of internal energy, i.e., the cooling of the neutral molecules is solely determined by the emission of thermal photons. Ultimately, this process determines the decoherence of the molecular wave since the thermal photons may carry which-path information.

A. The fullerene emission spectrum

The thermal radiation emitted from fullerenes was observed to have a continuous spectrum [13]. However, the spectral emission rate deviates from the Planck law of a macroscopic blackbody for a number of reasons. First, the radiating particle is much smaller than the typical photon wavelengths which indicates that it must be a colored emitter. The oscillator strengths of the available transitions can be related to the frequency-dependent absorption cross section [25]. Second, at the internal energies where thermal emission is relevant the particle is not in thermal equilibrium with the ambient radiation field so that there is no induced emission. Third, the emitter is not kept at a constant temperature, but the emission takes place at a fixed energy E . Similar to Einstein's derivation of the Planck law these aspects lead to the expression [26]

$$R_{\omega}(\omega, T)d\omega = \frac{\omega^2}{\pi^2 c^2} \sigma_{\text{abs}}(E(T) - \hbar\omega; \omega) \times \exp\left[-\frac{\hbar\omega}{k_B T} - \frac{k_B}{2C_V} \left(\frac{\hbar\omega}{k_B T}\right)^2\right] d\omega. \quad (1)$$

The first term is proportional to the mode density. The second term, the absorption cross section at internal energy $E(T) - \hbar\omega$ and frequency ω , quantifies the strength of the available electronic transitions. We disregard the temperature dependence of σ_{abs} since the relevant optical transitions have much higher energies than the thermal excitations. The third term in Eq. (1), the statistical factor, contains the first-order correction due to the finite heat capacity C_V of the fullerenes

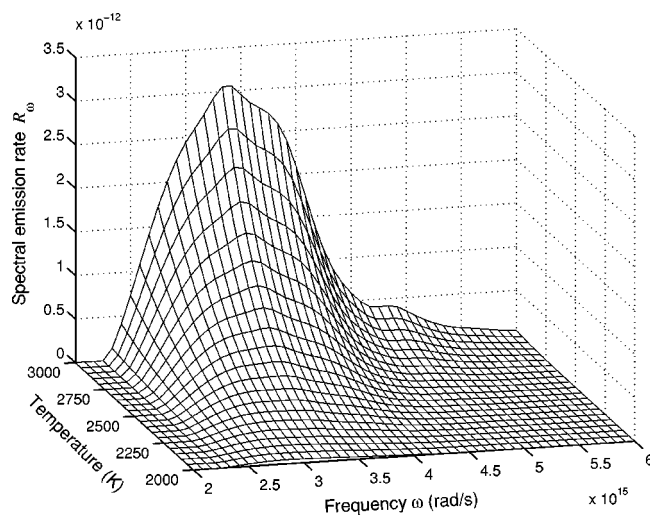


FIG. 4. The calculated spectral photon emission rate for (micro-canonical) molecular temperatures between 2000 and 3000 K; cf. Eq. (1). It involves a measured frequency-dependent absorption cross section [28]. The data imply that about three visible photons are emitted during a transit time of 4 ms.

[14,26]. It takes into account that the photon emission occurs at a fixed total energy rather than at a fixed temperature.

The heat capacity of C_{70} is practically constant at temperatures between 1000 and 3000 K [27]. It was calculated from the energies of the vibrational levels to be about $C_V = 202k_B$.

Using measured data for the absorption cross section [28] we obtain the spectral emission rate shown in Fig. 4. It is given for the temperature range between 2000 and 3000 K that is relevant in our experiment and covers the range of visible frequencies. Note that there are no contributions in the infrared because of a lack of accessible transitions below 1.6 eV, the energy of the gap between the highest occupied and lowest unoccupied molecular orbitals in the molecule [20]. Although some of the 204 vibrational modes of C_{70} are radiative in the far infrared [20], they do not contribute appreciably to decoherence or cooling in our experiment since the corresponding transition matrix elements are extremely small [29]. The small bump that can be seen at large temperatures around $\omega = 4.8 \times 10^{15}$ rad/s corresponds to the energy of 3.16 eV belonging to the first allowed dipole transition. The other direct dipole transitions and the plasma resonance at greater energies are still suppressed below 3000 K by the Boltzmann factor in Eq. (1).

B. The cooling dynamics

The radiative cooling of the fullerene molecules is determined by the spectral emission rate through the total radiant flux

$$\Phi(T) = \int_0^\infty \hbar \omega R_\omega(\omega, T) d\omega. \quad (2)$$

It is important to note that the temperature dependence of Φ differs considerably from the Stefan-Boltzmann law in the

case of fullerenes, due to the gap in the electronic excitation spectrum mentioned above. Indeed, from Eqs. (1) and (2) one finds that the radiant flux of C_{70} is given approximately by $\Phi(T) = 6.3 \times 10^{-35} [T/(K)]^{11}$ eV/s in the temperature regime of $T = 2000$ – 3000 K which will be relevant below. It shows that the thermal emission of fullerenes increases much more strongly with temperature than the well-known T^4 dependence of a blackbody.

It follows that the temporal evolution of a hot, neutral fullerene is governed by the cooling equation

$$\frac{d}{dt} T(t) = - \frac{\Phi(T)}{C_V}. \quad (3)$$

By integrating Eq. (3) numerically for a finite time $t > 0$ we find that the reduction of an initial temperature T_0 is described extremely well by the approximate formula

$$T(t; T_0) = T_0 \left[1 + \left(\frac{T_0}{T_\infty} \right)^n \right]^{-1/n}, \quad (4)$$

with the time-dependent parameters n and T_∞ . From this it follows that an initial temperature distribution $f_0(T)$ transforms as

$$f_t(T) = f_0 \left(T \left[1 - \left(\frac{T}{T_\infty} \right)^n \right]^{-1/n} \right) \left[1 - \left(\frac{T}{T_\infty} \right)^n \right]^{-(n+1)/n}. \quad (5)$$

Note that any temperature distribution will be bounded from above after a finite time by the maximum temperature T_∞ , as implied by Eq. (4).

The parameters n and T_∞ are obtained by fitting the function (4) to the numerical solution of Eq. (3). For the short times of flight t between the heating beams we find $n = 6.2$, $T_\infty = 830$ K $\times [(s)/t]^{1/n}$. The longer passage from the heating beams to the first grating of the interferometer is characterized by $n = 8.5$ and $T_\infty = 1700$ K $\times [v (s/m)]^{1/n}$, with v the velocity. During the long flight from the first grating to the detection laser the cooling is described by $n = 10.5$, $T_\infty = 2166$ K for a fullerene velocity of 100 m/s, and by $n = 9.7$, $T_\infty = 2321$ K for 190 m/s, respectively. Finally, we have $n = 9$, $T_\infty = 1490$ K $\times [v (s/m)]^{1/n}$ for the range of about 30 cm behind the detection laser where ions are recorded.

IV. MOLECULAR THERMOMETRY: THEORETICAL DESCRIPTION

After the fullerene beam has passed the heating stage it is no longer characterized by a single internal temperature. Rather, it shows a distribution of temperatures because of the stochastic nature of the photon absorption and as a result of the different heating intensities seen by the fullerenes due to the laser beam profiles. The resulting average temperature cannot be measured directly with a spectrometer since there are too few detectable photons emitted while the fullerenes travel through the interferometer. Instead, we have to resort to an indirect assessment of the temperature distribution.

The beam temperature is inferred in our experiment from an accurate measurement of the molecular ions, which appear due to the thermal emission of electrons from the hot

fullerenes in the heating stage. They are recorded as a function of the fullerene velocity, the laser power, and the number of heating laser beams. By comparing a model calculation to many experimental curves we obtain reliable information on the temperature distribution in the beam. A second, independent source of information is the count rate variation in the final molecule detector. This is because the fullerenes carry much of their added energy through the whole interferometer and their temperature determines the final detection efficiency. As discussed below, our model calculation also reproduces the experimental detection rate for different heating powers and fullerene velocity, which confirms independently the implied temperature distribution.

A quantitative description of the heating dynamics and the resulting ion signal faces several challenges. First, the photon absorption is a stochastic process giving rise to an initially broad distribution of temperatures in the beam. Second, there is a delicate competition between radiative emission and ionization, which both depend in a strong and nonlinear fashion on the fullerene temperature. Third, the radiative cooling of the molecules between the subsequent heating laser beams must also be taken into account. Finally, the description is further complicated by the fact that the fullerenes experience different heating intensities due to the finite extension of the molecular and optical beams. In the following model all those aspects are taken into account, which is necessary to provide a realistic description of the experimental situation.

We represent the initial velocity distribution by the function [30]

$$i_{C70}(v)dv = C_T v^3 \exp\left(-\frac{v^2}{v_w^2}\right)dv, \quad (6)$$

corresponding to an effusive molecular beam. Here $v_w = \sqrt{2k_B T/m} = 133$ m/s is the most probable speed of the C_{70} molecules in the oven and C_T a constant determined by the oven aperture. We then introduce the nonionized fraction $i_{C70}(v, z)$ of the beam at longitudinal position z and fullerene velocity v . Moreover, we need the distribution $i_{C70}(T, y; v, z)$ of the nonionized fraction with respect to the molecular temperature T , and the vertical position y . Initially, the distribution is peaked in T at 900 K, flat in y , and normalized, $\int dy \int dT i_{C70}(T, y; v, 0) = 1$. In terms of this quantity the current of neutral fullerenes at longitudinal position z is given by

$$i_{C70}(v; z) = C_T v^3 \exp\left(-\frac{v^2}{v_w^2}\right) \int dy \int_0^\infty dT i_{C70}(T, y; v, z). \quad (7)$$

The evolution of the distribution of the neutral fraction i_{C70} contains all the information needed to extract the observable ion yield and detection efficiency. We calculate the dynamics of i_{C70} by sequences of transformations which describe the heating experienced by crossing a single laser beam and the subsequent cooling and ionization.

In doing so we allow for an absorption cross section σ_{abs} in the metastable T_1 state which may differ from the ground state absorption cross section. At the same time only sequential absorption is considered, since the neglect of multiphoton effects is certainly justified at the prevailing laser intensities.

The absorption of laser photons is determined by a Poissonian probability distribution. Every green photon adds 2.3 eV to the molecule and therefore increases the temperature by $\Delta T = \hbar \omega_L / C_V = 139$ K. Correspondingly, each passage through a single laser beam changes the distribution in the fullerene beam according to

$$i'_{C70}(T, y; v, z_L) = e^{-\bar{n}(v, y)} \sum_{n=0}^{\infty} \frac{[\bar{n}(v, y)]^n}{n!} i_{C70}(T - n\Delta T, y; v, z_L). \quad (8)$$

The mean number of absorbed photons follows from an integration over the Gaussian laser mode centered at y_0 . It is given by

$$\bar{n}(v, y) = \sqrt{\frac{2}{\pi}} \frac{\lambda \sigma_{\text{abs}}}{\pi h c w_y v} P \exp\left(-\frac{2(y - y_0)^2}{w_y^2}\right). \quad (9)$$

The cooling and ionization processes after the heating are governed by Eq. (4) and by the Arrhenius law¹

$$\frac{d}{dz} i_{C70}(T, y; v, z) = -\frac{A_{\text{ion}}}{v} \exp\left(-\frac{E_{\text{ion}}}{k_B T}\right) i_{C70}(T, y; v, z). \quad (10)$$

In our case the ionization energy is to be taken from the triplet state T_1 , that is $E_{\text{ion}} = 7.6$ eV – 1.6 eV. Since the evolution of the temperature $T(z/v; T_0)$ is known explicitly (4) one can integrate Eq. (10). This way we obtain

$$\begin{aligned} i_{C70}(T, y; v, z + \Delta z) \\ = i_{C70}\left(T\left(1 - \frac{T^n}{T_\infty^n}\right)^{-1/n}, y; v, z\right) \left(1 - \frac{T^n}{T_\infty^n}\right)^{-(n+1)/n} \\ \times \exp\left[-\frac{A_{\text{ion}} L}{v} C\left(v, T\left(1 - \frac{T^n}{T_\infty^n}\right)^{-1/n}\right)\right] \end{aligned} \quad (11)$$

with

$$\begin{aligned} C(v, T_0) = n \frac{T_\infty^n(v)}{T_{\text{ion}}^n} \left[\Gamma\left(n, \frac{T_{\text{ion}}}{T_0}\right) \right. \\ \left. - \Gamma\left(n, \frac{T_{\text{ion}}}{T_0} \left(1 + \frac{T_0^n}{T_\infty^n(v)}\right)^{1/n}\right) \right]. \end{aligned} \quad (12)$$

Here $\Gamma(n, x)$ is the incomplete gamma function and $k_B T_{\text{ion}} = E_{\text{ion}}$. Equation (11) describes the reduction of the neutral fraction and its temperature variation during a free flight under the joint action of radiative cooling and ionization.

¹In the literature there are also proposals for a slightly different form of the Arrhenius law for fullerenes [31]. We checked that the result of our calculation described below does not depend significantly on the precise temperature dependence of the ionization rate.

The transformations (8) and (11) are applied as often as there are intersecting laser beams, which have an average separation of 0.3 mm. We take their vertical positions to be uniformly distributed within a width of about $1.5w_y$, which is the estimate obtained from the experimental beam alignment. Our values for $T_\infty(v)$ and n are given above in Sec. III.

The ion yield in the heating region, which is measured at detector D_1 , is given by the change in the current of neutral molecules. It reads

$$I(v) = C_T v^3 \exp\left(-\frac{v^2}{v_w^2}\right) \int dy \int_0^\infty dT [i_{C70}(T, y; v, 0) - i_{C70}(T, y; v, z_{G1})]. \quad (13)$$

Here we account also for possible delayed ionization by extending the measurement interval to the interferometer entrance z_{G1} . However, delayed ionization does not play an important role for the parameters given below, and virtually no ionization is predicted for $z > z_{G1}$.

The final detection stage D_2 also operates by laser-induced thermionic emission. Therefore, one can calculate its temperature- and velocity-dependent detection efficiency using Eqs. (8) and (11) as well. We use the values given in Sec. II B for the wavelength of the detection laser and its waist, and take the maximal ionization distance to be 30 cm.

V. MOLECULAR THERMOMETRY: EXPERIMENTAL RESULTS

In order to gauge our heating setup we measure the ionization yield in the heating stage. Positive ions are accelerated to the conversion dynode where they release secondary electrons which are in turn accelerated to a secondary electron multiplier situated 1 cm above the conversion plate. The first heating beam was adjusted such that its focus is lying just below the rim of the channeltron. This setup ensures that the observed electric signal is essentially proportional to the ion current produced in the heating region.

We use a chopped molecular beam and a time-of-flight sensitive detection scheme to measure the velocity of the neutral fullerenes, which determines the heating time. In addition, the number of heating beams can be varied by blocking the laser beam after a specified number of reflections. This way the normalized ion yield $I(v)/[C_T v^3 \exp(-v^2/v_w^2)]$ could be extracted as a function of the fullerene velocity, the heating power, and for heating configurations with four and with ten crossing beams; see Fig. 5.

The corresponding model calculation depends on two unknown parameters, the absorption cross section in the triplet state $\sigma(T_1)$ and the Arrhenius constant for ionization A_{ion} . By comparing simultaneously the various measured ion curves to the model we extract the common fit values $\sigma(T_1) \approx 2 \times 10^{-17} \text{ cm}^2$ and $A_{\text{ion}} \approx 5 \times 10^9 \text{ s}^{-1}$. Our value for the cross section $\sigma(T_1)$ is close to that of the known ground state absorption cross section [28]. This is reasonable with C_{70} , where the dipole matrix elements have fewer symmetry restrictions than C_{60} . We did not find published Arrhenius constants for C_{70} , but we note that the literature values for C_{60} vary by many orders of magnitude [32]. Given this it seems

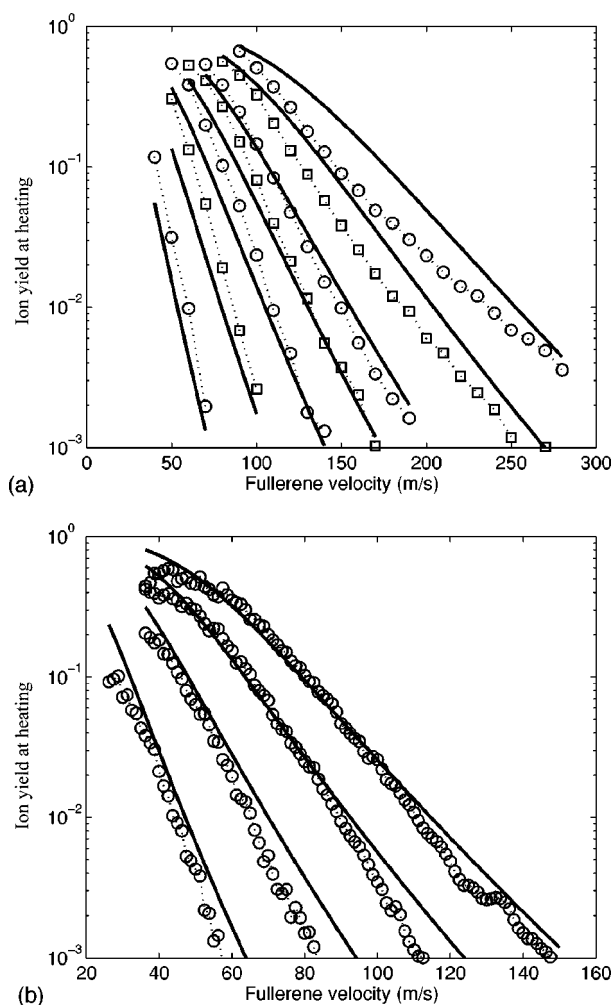


FIG. 5. Ion yield at the heating stage; experimental data (symbols) compared to the model calculation (solid lines). Top: Arrangement with ten heating beams and laser powers of $P=2, 3, 4, 5, 6, 8, 10$ W. Curves with higher count rates are associated with higher laser powers. Bottom: Arrangement with four heating beams and laser powers of $P=4, 6, 8, 10$ W.

acceptable that our value is smaller than the range of literature values for C_{60} . Figure 5 shows the experimental data for the ion yield along with the results of the model calculation using the mentioned parameters.

In addition to the above measurements, we also record the change of the count rate in the final detection stage as a function of the heating power, the number of heating beams, and for two different fullerene velocities of 100 and 190 m/s. The experimental data are shown in Fig. 6. They are compared to the model calculation using the *same* parameters as above, and one observes a good agreement of the various curves. This is strong evidence that the model succeeds in describing the relevant cooling and ionization processes. It serves also to explain the form of the experimental data curves. The increase in the detection rate at small heating powers is due to the higher temperature of the fullerenes arriving at the detection stage. The increased internal energy raises the ionization probability after crossing the detection laser beam. This effect is superseded at higher heating pow-

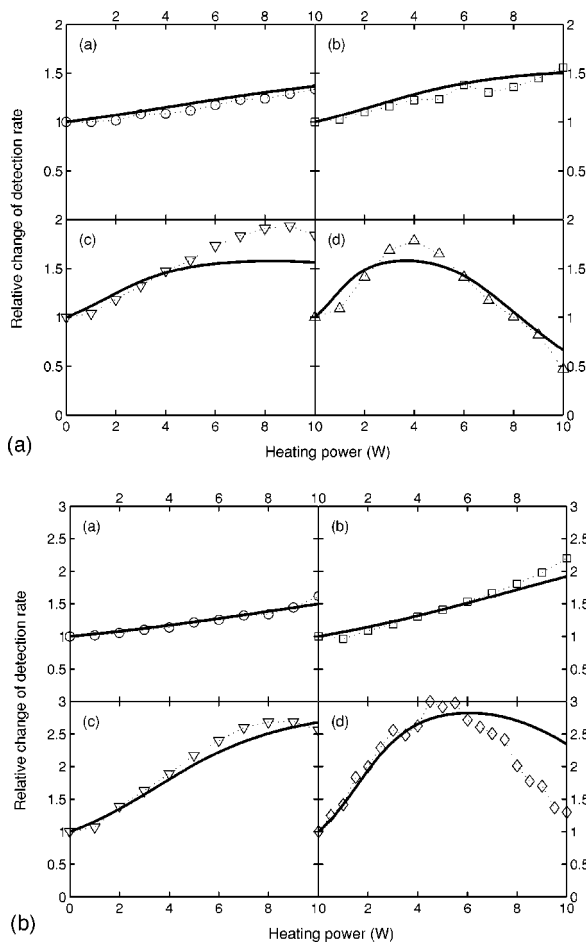


FIG. 6. Relative change of the molecular detection rate at D_2 as a function of the heating laser power. Experimental data (symbols) vs model calculation (solid lines). Top: Fullerenes with 100 m/s. The number of heating beams was (a) one, (b) two, (c) four, and (d) ten. Bottom: Faster fullerenes with a velocity of 190 m/s and (a) two, (b) four, (c) ten, and (d) 16 heating beams.

ers and a large number of heating beams by a reduction of the detection rate. It is due to the fact that at strong heating a sizable fraction of the fullerene beam is ionized already in the heating stage.

The good agreement of the described measurements with the model calculation leads us to conclude that the model provides a realistic description of the temperature evolution in the beam. Figure 7 shows the implied temperature distribution in the beam directly after heating and at the position of the first grating. The fullerene velocities are taken to be 100 and 190 m/s corresponding to the experimental choice for observing the first and second Talbot orders. Note that the slower molecules, which are heated more strongly, arrive at the first grating with a smaller temperature on average because they have more time of flight to cool off.

A final remark concerns the dependence of the model calculation on the fit parameters $\sigma(T_1)$ and A_{ion} which were obtained from the curves in Fig. 5. While the ionization and detection curves show a moderate dependence on these parameters, the temperature distribution given in Fig. 7 is very robust. The reason is that only the absorption cross section

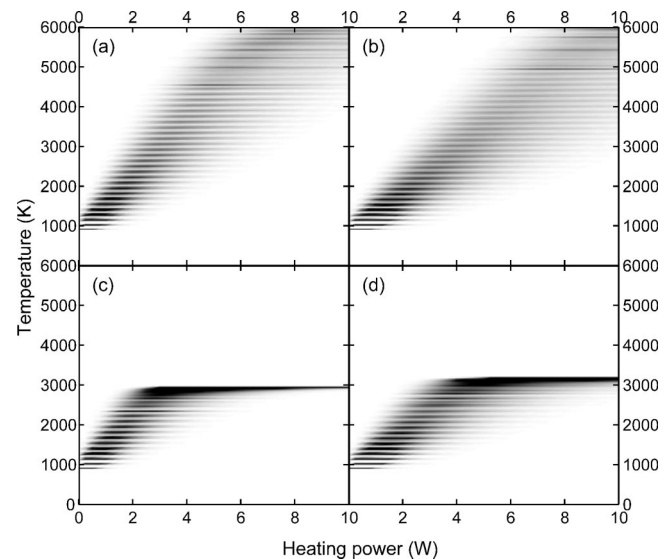


FIG. 7. Temperature distributions in the beam implied by our model calculation directly after the heating stage (a),(b) and at the position of the first grating (c),(d). The shading is proportional to the probability density of the temperature. The data are shown for a fullerene velocity of 100 m/s (a),(c) and of 190 m/s (b),(d), respectively. The stripes in (a) and (b) correspond to the temperature increase $\Delta T=139$ K due to a single photon absorption. The stripes are somewhat closer in (c) and (d) due to cooling.

$\sigma(T_1)$ enters in this figure, which is much better specified by the fitting procedure than A_{ion} . Incidentally, only this robust temperature distribution enters the calculation in the following treatment of radiative decoherence.

VI. DECOHERENCE BY THERMALLY EMITTED RADIATION

The effect of the molecular temperature on the wave nature of the fullerenes can now be measured using the Talbot-Lau interference effect described in Sec. II A. The “fast” fullerenes with $v=190$ m/s correspond to the first-order Talbot effect. They are heated by an arrangement of 16 laser beams. Ten beams are used for the slower fullerenes that are required for the second Talbot order ($v=100$ m/s).

Figure 8 shows the observed interference fringes of the fast molecules for various heating powers. The variation of the mean count rate is discussed in Sec. V. We use sinusoidal fits (the solid lines) in order to extract the visibility $V = (I_{\text{max}} - I_{\text{min}}) / (I_{\text{max}} + I_{\text{min}})$, which is a direct measure of the particle’s wave nature.

According to decoherence theory, the ability of a hot object to show interference is limited by the rate and wavelengths of the thermally emitted photons. A detailed description of the theoretical treatment of decoherence in the Talbot-Lau interference has been given in Ref. [14]. It predicts the reduction of the fringe contrast due to the emission of thermal photons, in particular for the sinusoidal fringes observed in our symmetric Talbot-Lau interferometer. For a molecule with the initial temperature T_0 and a velocity v the reduction factor is given by

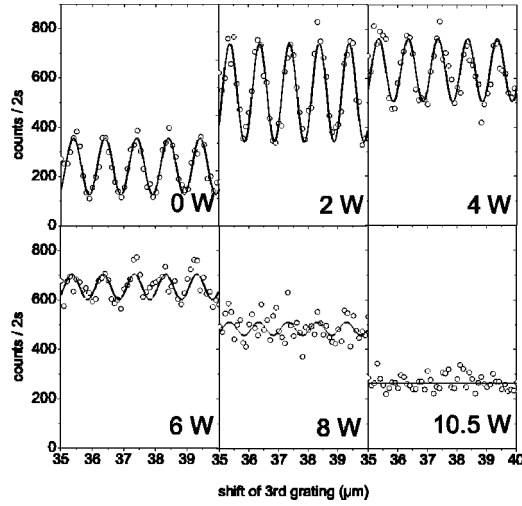


FIG. 8. Fullerene interference fringes corresponding to the first-order Talbot-Lau effect at different powers of the heating laser. The stronger the heating in front of the interferometer the more thermal radiation is emitted within the interferometer, leading to a monotonic reduction of fringe contrast. The variation of the mean absolute count rate is caused by the thermal ionization detection scheme. While it is irrelevant for the assessment of the degree of coherence, it provides us with a second method for the evaluation of the molecular temperature, as discussed in the text and indicated in Fig. 6. The solid curves are sinusoidal fits used to extract the fringe visibility.

$$R(T_0, v) = \exp \left\{ - \int_0^{2L/v} dt \int_0^\infty d\omega R_\omega(\omega, T(t; T_0)) \times \left[1 - \operatorname{sinc} \left(\frac{\omega d L - |vt - L|}{c L_T} \right) \right] \right\}. \quad (14)$$

Here, $R_\omega(\omega, T)$ is the spectral photon emission rate (1) at angular frequency ω and temperature T . The function $T(t; T_0)$ gives the temporal variation of the fullerene temperature. The argument of the function $\operatorname{sinc}(x) = \sin(x)/x$ compares the wavelength $\lambda = 2\pi c/\omega$ of the thermal photon to the effective separation of the contributing interfering paths.

Equation (14) is most intuitive for first- (second-) order Talbot interference where the grating distance L equals (equals twice) the Talbot length $L_T = d^2/\lambda_{C70}$. Then, the photon wavelength gets compared to the actual separation of paths running through neighboring slits (next to neighboring slits) in the central grating.

It should be noted that the change of the *internal* fullerene state upon photon emission does not matter for decoherence. The reason for this is that the internal degrees of freedom do not get entangled with the center-of-mass coordinate, since the emission probability is position independent.

The precise form of the spectral photon emission rate R_ω for C_{70} fullerenes and their temperature evolution were discussed in Sec. III. In order to predict the expected loss of interference contrast one needs to account for the temperature distribution shown by the fullerenes when they enter the interferometer. It is given by

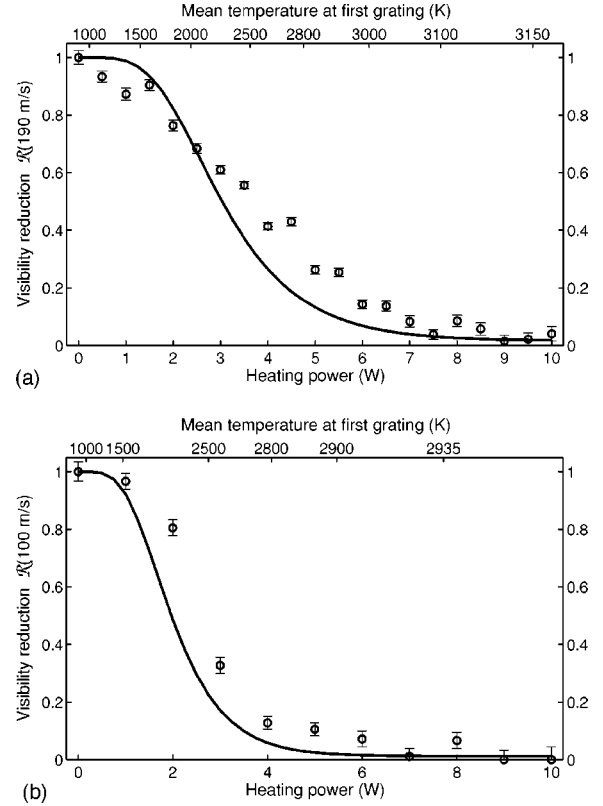


FIG. 9. Reduction of the interference visibility due to heating with laser power P . The circles give the experimental visibility extracted from fringe patterns such as shown in Fig. 8; the solid lines are the theoretical expectation given by Eq. (16). The fullerenes in the top graph have a velocity of 190 m/s corresponding to the first Talbot order, while in the bottom graph the fullerene velocity is 100 m/s corresponding to the second Talbot order. The upper scale gives the mean fullerene temperature at the entrance of the interferometer.

$$f_{G1}(T; v) = \int dy i_{C70}(T, y; v, z_{G1}) \quad (15)$$

since the vertical position is irrelevant in the interferometer. The expected visibility reduction is calculated by weighting the reduction factor (14) with this distribution.

$$\mathcal{R}(v) = \int dT_0 f_{G1}(T_0; v) \mathcal{R}(T_0, v). \quad (16)$$

We use a numeric integration of (3) in order to evaluate the required function $T(t; T_0)$.

It turns out that the cooling within the interferometer contributes to the quantitative prediction of the interference contrast. The visibility loss due to emissions in the first half of the symmetric interferometer is in general much stronger than in the second half. At the same time, Eq. (1) predicts that unheated molecules, thermalized only to the oven temperature of 900 K, do not cool or decohere noticeably during their time of flight in the apparatus.

As discussed in Sec. III the spectral emission rate of fullerenes deviates considerably from the Boltzmann law of

a blackbody. This is one of the reasons why the simple estimates of temperature effects in Refs. [33–35] cannot be used to describe the experiment. Similarly, the more recent studies in Refs. [36,37] do not apply to the present experimental situation.

The visibilities extracted from the experimental fringe patterns are given in Fig. 9, where they are compared to the theoretical expectation (16). The error bars of the experimental data indicate only the statistical error of the visibility extraction. A much larger systematic error is due to the imperfections in the alignment of the heating laser beams. As a result, the variation of the experimental data after different alignments is of the order of the difference between the data shown and the experimental curve. Note that the upper scale in Fig. 9 gives the mean temperature in the beam at the entrance of the interferometer.

VII. DISCUSSION

The good agreement between experiment and decoherence theory found in Fig. 9 provides strong evidence for the observation of thermal decoherence. However, since the temperature measurement is indirect it is necessary to discuss the possibility of other laser-induced decoherence mechanisms that might give rise to a similar observation.

A different source of decoherence would ensue if the fullerenes were still in the electronic triplet state when they

enter the interferometer. This state is associated with a magnetic moment and arguably also with a higher electric polarizability. The molecules could therefore be slightly more susceptible to interactions with electromagnetic stray fields.

However, if this interaction were relevant one would expect a different relation between the interference fringe contrast and the heating laser power than it is observed in the experiment. A single absorbed photon would suffice to take the fullerene into the first excited triplet state with a probability of more than 90%. Correspondingly, we would expect a sharp threshold in the contrast curve of Fig. 9 when the laser power is increased. Moreover, we expect that the T_1 lifetime and therefore also its population in the interferometer should decrease with increasing heating power.

From the gradual decay of the visibility curve we can therefore safely exclude any effect that requires a nonthermal population of the excited state for the explanation of the observation.

ACKNOWLEDGMENTS

We acknowledge contributions by Björn Brezger at an early stage of the work, and we thank Anton Zeilinger for his continuous and helpful support. This work was supported by the Austrian FWF in the programs START Y177 and SFB F1505, by the European Union within the project HPRN-CT-2002-00309, and by the Emmy-Noether program of the Deutsche Forschungsgemeinschaft.

-
- [1] M. S. Chapman, C. R. Ekstrom, T. D. Hammond, R. A. Rubenstein, J. Schmiedmayer, S. Wehinger, and D. E. Pritchard, *Phys. Rev. Lett.* **74**, 4783 (1995).
 - [2] W. Schöllkopf and J. Toennies, *J. Chem. Phys.* **104**, 1155 (1996).
 - [3] C. Bordé, N. Courtier, F. D. Burck, A. Goncharov, and M. Gorlicki, *Phys. Lett. A* **188**, 187 (1994).
 - [4] W. Schoellkopf, R. Grisenti, and J. Toennies, *Eur. Phys. J. D* **28**, 125 (2004).
 - [5] M. Arndt, O. Nairz, J. Voss-Andreae, C. Keller, G. V. der Zouw, and A. Zeilinger, *Nature (London)* **401**, 680 (1999).
 - [6] L. Hackermüller, S. Uttenthaler, K. Hornberger, E. Reiger, B. Brezger, A. Zeilinger, and M. Arndt, *Phys. Rev. Lett.* **91**, 090408 (2003).
 - [7] E. Joos, H. D. Zeh, C. Kiefer, D. Giulini, J. Kupsch, and I.-O. Stamatescu, *Decoherence and the Appearance of a Classical World in Quantum Theory*, 2nd ed. (Springer, Berlin, 2003).
 - [8] M. S. Chapman, T. D. Hammond, A. Lenef, J. Schmiedmayer, R. A. Rubenstein, E. Smith, and D. E. Pritchard, *Phys. Rev. Lett.* **75**, 3783 (1995).
 - [9] D. A. Kokorowski, A. D. Cronin, T. D. Roberts, and D. E. Pritchard, *Phys. Rev. Lett.* **86**, 2191 (2001).
 - [10] M. Brune, E. Hagley, J. Dreyer, X. Maître, A. Maali, C. Wunderlich, J. M. Raimond, and S. Haroche, *Phys. Rev. Lett.* **77**, 4887 (1996).
 - [11] P. Bertet, S. Osnaghi, A. Rauschenbeutel, G. Nogues, A. Auffeves, M. Brune, J. M. Raimond, and S. Haroche, *Nature (London)* **411**, 166 (2001).
 - [12] Y. Ji, Y. Chung, D. Sprinzak, M. Heiblum, D. Mahalu, and H. Shtrikman, *Nature (London)* **422**, 415 (2003).
 - [13] R. Mitzner and E. E. B. Campbell, *J. Chem. Phys.* **103**, 2445 (1995).
 - [14] K. Hornberger, J. E. Sipe, and M. Arndt, *Phys. Rev. A* **70**, 053608 (2004).
 - [15] L. Hackermüller, K. Hornberger, B. Brezger, A. Zeilinger, and M. Arndt, *Nature (London)* **427**, 711 (2004).
 - [16] B. Brezger, L. Hackermüller, S. Uttenthaler, J. Petschinka, M. Arndt, and A. Zeilinger, *Phys. Rev. Lett.* **88**, 100404 (2002).
 - [17] J. F. Clauser and S. Li, *Phys. Rev. A* **49**, R2213 (1994).
 - [18] D. Ding, J. Huang, R. N. Compton, C. E. Klots, and R. E. Haufler, *Phys. Rev. Lett.* **73**, 1084 (1994).
 - [19] O. Nairz, B. Brezger, M. Arndt, and A. Zeilinger, *Phys. Rev. Lett.* **87**, 160401 (2001).
 - [20] M. S. Dresselhaus, G. Dresselhaus, and P. C. Eklund, *Science of Fullerenes and Carbon Nanotubes*, 2nd ed. (Academic Press, San Diego, 1998).
 - [21] E. A. Rohlfing, *J. Chem. Phys.* **89**, 6103 (1988).
 - [22] P. Heszler, J. O. Carlsson, and P. Demirev, *Chem. Phys.* **107**, 10440 (1997).
 - [23] O. Nairz, M. Arndt, and A. Zeilinger, *J. Mod. Opt.* **47**, 2811 (2000).
 - [24] S. Matt, O. Echt, M. Sonderegger, R. David, P. Scheier, J. Laskin, C. Lifshitz, and T. D. Märk, *Chem. Phys. Lett.* **303**, 379 (1999).

- [25] H. Friedrich, *Theoretical Atomic Physics* (Springer, Berlin, 1998).
- [26] K. Hansen and E. E. B. Campbell, *Phys. Rev. E* **58**, 5477 (1998).
- [27] E. Kolodney, B. Tsipinyuk, and A. Budrevich, *J. Chem. Phys.* **102**, 9263 (1995).
- [28] P. F. Coheur, M. Carleer, and R. Colin, *J. Phys. B* **29**, 4987 (1996).
- [29] J. U. Andersen and E. Bonderup, *Eur. Phys. J. D* **11**, 413 (2000).
- [30] *Atomic and Molecular Beam Methods*, edited by G. Scoles, D. Bassi, U. Buck, and D. Lainé (Oxford University Press, Oxford, 1988), Vol. I.
- [31] C. E. Klots, *Chem. Phys. Lett.* **186**, 73 (1991).
- [32] A. Reinköster, U. Werner, N. M. Kabachnik, and H. O. Lutz, *Phys. Rev. A* **64**, 023201 (2001).
- [33] E. Joos and H. D. Zeh, *Z. Phys. B: Condens. Matter* **59**, 223 (1985).
- [34] M. Tegmark, *Found. Phys. Lett.* **6**, 571 (1993).
- [35] R. Alicki, *Phys. Rev. A* **65**, 034104 (2002).
- [36] P. Facchi, A. Mariano, and S. Pascazio, *Recent Res. Dev. Phys.* **3**, 1 (2002).
- [37] A. Viale, M. Vicari, and N. Zanghi, *Phys. Rev. A* **68**, 063610 (2003).